Journal of Zhejiang University-SCIENCE A (Applied Physics & Engineering) 2024 25(11):908-921
www.jzus.zju.edu.cn; www.springer.com/journal/11582
E-mail: jzus_a@zju.edu.cn

Research Article

https://doi.org/10.1631/jzus.A2300507

Design and performance study on adaptive sealing of a dry cabin for maintenance of submarine pipeline

Jin GUO[1,3], Xinghui TAN[1], Hai ZHU[1], Jiawang CHEN[4], Shidi JIN[1], Yuanjie CHEN[2], Jie CHEN[2], Ruiduo YIN[2]✉

[1]*Institute of Ocean Engineering and Technology, Zhejiang University, Zhoushan 316021, China*
[2]*Zhejiang Institute of Metrology, Hangzhou 310018, China*
[3]*Hainan Institute, Zhejiang University, Sanya 572025, China*
[4]*Donghai Laboratory, Zhoushan 316021, China*

Abstract: The underwater dry maintenance method based on a dry cabin can achieve the same maintenance quality provided on land. The establishment of a reliable seal between the dry cabin and the pipe is a prerequisite for the formation of a dry environment. In this paper, an airbag is proposed as the means to seal the dry cabin. ABAQUS finite element software was used to study the influence of the physical characteristics of the airbag on deformation characteristics and sealing performance. We also studied the adaptive sealing mechanism of the airbag under the time-varying gap condition. The simulation results show that the peak contact stress of the airbag is close to the gas pressure, so the hardness and thickness of the airbag have little effect on it. Under time-varying gap conditions, the required inflation pressure increases with the size of the gap. The simulated relationship between the gap and the inflation pressure can be referred to in order to guide the control of the air pressure of the airbag during actual operation. Finally, the similarity between the test results and simulation results demonstrates the accuracy of the simulation results.

Key words: Submarine pipeline; Underwater dry cabin; Silicone airbag; Sealing performance

1 Introduction

Submarine pipelines are the main components of offshore oil (gas) field development and production systems, and some submarine pipelines have been in service for more than 30 years (Animah and Shafiee, 2018). Compared with the land pipelines, the submarine pipelines are exposed to the harsh marine environment for a long time. Pipelines have great failure probability due to the multiple effects of metal corrosion (Yang et al., 2017), ocean-current erosion (Yang et al., 2017), natural disasters (Badida et al., 2019), and strikes from ships' anchors (Gucma and Zalewski, 2003).

The traditional repair methods for submarine pipelines are mainly sea-surface dry repair and underwater wet repair (Mao et al., 2015; Li et al., 2016; Drumond et al., 2018). Surface dry repair involves a high cost and heavy workload, and underwater wet repair results in poor welding quality. Therefore, the dry repair method based on a dry cabin has been proposed. Since the underwater dry inspection method is carried out in an air environment, it becomes possible to apply the same inspection process used on land on the seabed, thereby improving the same quality of inspection and repair. A subsea pipeline dry cabin is necessary to provide an underwater dry environment. The seawater inside the cabin is discharged to form a dry working environment, and the establishment of a reliable seal between the dry cabin and the pipe is a prerequisite for the formation of a dry environment. Existing underwater dry cabins are sealed mainly by compressing solid rubber strips. For example, the world's first underwater dry-welded

✉ Ruiduo YIN, 306964154@qq.com
Jin GUO, https://orcid.org/0000-0002-2726-5936
Xinghui TAN, https://orcid.org/0009-0004-4989-0590
Hai ZHU, https://orcid.org/0000-0002-4681-163X
Jiawang CHEN, https://orcid.org/0000-0002-6351-0062
Shidi JIN, https://orcid.org/0009-0008-6412-0438
Yuanjie CHEN, https://orcid.org/0009-0005-7276-6982
Jie CHEN, https://orcid.org/0009-0006-1413-9830
Ruiduo YIN, https://orcid.org/0009-0005-1512-2603

Received Oct. 7, 2023; Revision accepted Jan. 19, 2024;
Crosschecked Aug. 13, 2024; Online first Sept. 28, 2024

cabin (UWH) is sealed by squeezing rubber through hydraulic doors (Gaudiano, 1975; Fleury and Schofield, 1979; Pratt et al., 1997). In addition, some cabins rely on underwater frogmen to install steel plates to squeeze rubber for sealing, such as the underwater habitat clamp (UHC) (Berge et al., 2008; Vernon and Werner, 2009) and the habitat designed and built by DCN Diving, China (Tronskar and Lee, 2016; Lee Toups et al., 2021).

Meanwhile, inflatable airbags are a sealing method widely used in large-scale energy and infrastructure projects for the advantages of high filling degree, large deformation degree, and sealing on demand. Jiang et al. (2012) used a combination method of theory and experiment to study the stability and air-tightness of fast-sealing airbags in tunnels. By comparing and analyzing the heat resistance, flame retardant, wear resistance, hardness, and air permeability of different kinds of rubber, they identified the ideal fluoro rubber material. In order to effectively contain catastrophic accidents, Ma et al. (2022) designed a way to rapidly seal disaster areas with inflatable capsules. The dynamic response characteristics of a small inflatable airbag under an explosion shock wave were studied. To build a device to quickly close a pipeline in the event of explosion propagation and/or chemical leakage, Eisenreich et al. (2007) built an airbag capable of withstanding a pressure of up to 1 MPa. The modeling and shape analysis of the airbag in the pipeline were completed with computational fluid dynamics (CFD) technology.

In order to improve the sealing performance of such an airbag, some studies have examined the parameters that affect it. Dong et al. (2021) used experimental and simulation methods to study the effects of airbag location, height, and thickness of oil- and gas-pipeline cleaning balls on multi-airbag sealing-disc bending angles and airbag expansion ratios. Chen et al. (2019) discussed and optimized the relationship between inflation rate and airbag parameters (volume and pressure) by using common coupling surface analysis in MSC Dytran finite element software. Given the current problems with the stability and air tightness of fast-sealing airbags, Jiang et al. (2012) completed the optimal selection of an airbag by comparing and analyzing the heat resistance, flame retardance, wear resistance, hardness, and air permeability of different types of rubber. After studying the stress characteristics and failure mechanism of conventional airbags, Chen et al. (2023) put forward a method to improve the blocking ability of conventional airbags through reinforcement. They established a force-analysis model of reinforced airbags under external pressure, revealed the reinforcement mechanism, and obtained the calculation formula for critical external pressure.

In this study, we used ABAQUS finite element software to study the effect of the physical characteristics of an airbag on its sealing performance. We also investigated the adaptive sealing mechanism under time-varying gap conditions. The specific work was as follows: (1) uniaxial tests were carried out to obtain the stress–strain constitutive model of a silica gel airbag; (2) ABAQUS was used to analyze the sealing and force characteristics of sealing airbags with five kinds of cross-section shapes; (3) under the constant-gap working conditions, the influences of material hardness, wall thickness, and inflation pressure on the deformation, mechanical, and sealing characteristics of the airbag were studied; (4) the sealing characteristics of the selected airbag were studied under time-varying gap conditions, and the adaptive sealing mechanism of the airbag was evaluated; (5) a full-scale airbag pressure test was carried out to verify the rationality of the simulation results.

2 Objects to be sealed: dry cabin for subsea pipeline maintenance

Fig. 1 shows the dry cabin developed by our team for subsea pipeline inspection and repair. As shown in

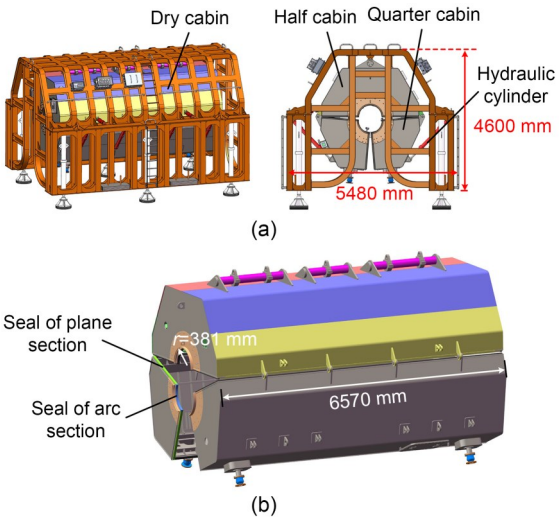

Fig. 1 (a) Diagram of the dry cabin; (b) schematic diagram of the sealing type of the dry cabin

Fig. 1a, the cabin consists of a top-half cabin and two bottom-quarter cabins. The quarter cabin is hinged and fixed on the half cabin, and the opening and closing of the cabin are realized under the action of a hydraulic cylinder. The working depth of the dry cabin is less than 40 m. The working principle is to establish a seal between the dry cabin and the pipeline after the dry cabin is closed, and then the water in the dry cabin is pumped out and the cabin is filled with high-pressure gas to form a dry environment. As shown in Fig. 1b, the sealing of dry cabins can be divided into two stages. The first stage is sealing the plane section between the half and quarter cabins, as marked in Fig. 1b. The second stage is sealing the arc section between the dry cabin and the pipeline, as marked in Fig. 1b. The sealing of the arc section is accomplished with a combination of ethylene propylene diene methylene (EPDM) foam material and an inflatable airbag. When the pipe has a bend angle, the arc section of the dry cabin is not coaxial with the pipe (that is, the pipe appears eccentric), resulting in uneven compression of the seal strip in the arc section. In order to solve the problem of seal failure caused by the poor adaptive performance of EPDM foam material, we propose an adaptive seal between the dry cabin and the pipe. The sealing properties of EPDM foams have been discussed in detail in our previous study (Guo et al., 2024). Therefore, this paper mainly discusses the sealing characteristics of airbags. The airbag is supplied with gas through an air compressor unit on the deck. As there is no specific standard for the selection and design of airbag seals, it was necessary to study the factors that affect airbag seal performance.

The sealing of the dry cabin is mainly achieved through the use of EPDM sealing strips, which have good resistance to damage. Airbags are only used to compensate for some gaps. Therefore, damage to the airbags will not lead to accidents, only to leaks.

3 Methods

3.1 Silica gel stress–strain constitutive model and seal-failure judgment criteria

The mechanical analysis of silica gel, a hyperelastic material, cannot be described only in terms of elastic modulus and Poisson's ratio like linear elasticity. Instead, the stress–strain data of silica gel airbags must be obtained by the uniaxial test, and the coefficient of the material constitutive model can be obtained by fitting the test data. One effective theory to describe the characteristics of hyperelastic materials is the constitutive theory based on the strain energy–density function.

In this study, we used the two-parameter Mooney-Rivlin hyperelastic model for nonlinear finite element analysis (Mooney, 1940; Rivlin, 1948; Rivlin and Saunders, 1951):

$$W=c_{10}(\bar{I}_1-3)+c_{01}(\bar{I}_2-3)+\frac{1}{d}(J-1)^2, \tag{1}$$

where W is the strain energy potential, c_{10} and c_{01} are the material constants characterizing the material deflection, $\bar{I}_1$ and $\bar{I}_2$ are the first and second partial strain invariants, respectively, J is the determinant of the elastic deformation gradient, and d is the material incompressibility parameter. The expression is as follows:

$$d=\frac{1-2\mu}{c_{10}-c_{01}}, \tag{2}$$

where μ is Poisson's ratio.

From the relationship between the Kirchoff stress tensor $\boldsymbol{t}_{ij}$ and Green strain tensor $\boldsymbol{\gamma}_{ij}$:

$$\boldsymbol{t}_{ij}=\frac{\partial W}{\partial \bar{I}_1}\frac{\partial \bar{I}_1}{\partial \boldsymbol{\gamma}_{ij}}+\frac{\partial W}{\partial \bar{I}_2}\frac{\partial \bar{I}_2}{\partial \boldsymbol{\gamma}_{ij}}+\frac{\partial W}{\partial \bar{I}_3}\frac{\partial \bar{I}_3}{\partial \boldsymbol{\gamma}_{ij}}. \tag{3}$$

The relationship between the principal stress σ_i of rubber material and its principal elongation ratio λ_i is as follows:

$$\sigma_i=2\left(\lambda_i^2\frac{\partial W}{\partial \bar{I}_1}+\frac{1}{\lambda_i^2}\frac{\partial W}{\partial \bar{I}_2}\right)+P, \tag{4}$$

where P is the hydrostatic pressure.

Three principal stress differences can be obtained from the above equation:

$$\begin{aligned}
\sigma_1-\sigma_2&=2(\lambda_1^2-\lambda_2^2)\left(\frac{\partial W}{\partial \bar{I}_1}+\lambda_3^2\frac{\partial W}{\partial \bar{I}_2}\right),\\
\sigma_2-\sigma_3&=2(\lambda_2^2-\lambda_3^2)\left(\frac{\partial W}{\partial \bar{I}_1}+\lambda_1^2\frac{\partial W}{\partial \bar{I}_2}\right),\\
\sigma_3-\sigma_1&=2(\lambda_3^2-\lambda_1^2)\left(\frac{\partial W}{\partial \bar{I}_1}+\lambda_2^2\frac{\partial W}{\partial \bar{I}_2}\right).
\end{aligned} \tag{5}$$

For unidirectional tension or compression, $\sigma_2=\sigma_3=0$, $\lambda_2^2=\lambda_3^2=1/\lambda_1$, then

$$\sigma_1=2\left(\lambda_1^2-\frac{1}{\lambda_1}\right)\left(\frac{\partial W}{\partial \bar{I}_1}+\frac{1}{\lambda_1}\frac{\partial W}{\partial \bar{I}_2}\right). \tag{6}$$

Based on Eq. (1), Eq. (7) can be obtained:

$$\frac{\partial W}{\partial \bar{I}_1}=C_{10},\quad \frac{\partial W}{\partial \bar{I}_2}=C_{01}. \tag{7}$$

Substituting Eq. (7) into Eq. (6), we can obtain:

$$\frac{\sigma_1}{2\left(\lambda_1^2-\frac{1}{\lambda_1}\right)}=C_{10}+\frac{1}{\lambda_1}C_{01}. \tag{8}$$

The above equation is the basic formula for determining C_{10} and C_{01} by uniaxial tensile or compression test.

The criterion for seal failure is to compare the relationship between the maximum contact stress and the working stress. When the maximum contact stress is greater than the working pressure, it is considered that the seal has not failed.

3.2 Simulation model and mesh division

In light of the uniform distribution of the geometric configuration and load attributes along the circumference of the arc section, we have transformed the complex 3D model into a more manageable 2D counterpart, focused solely on a singular cross-section. Furthermore, with respect to voluminous dry cabins, the transition to the 2D model serves to mitigate the overarching burden of modeling, whilst simultaneously decreasing the time required for simulation computations.

The Mooney-Rivlin hyperelastic model describing rubber elastic deformation was provided by ABAQUS finite element software, which has been widely used in sealing research (Cui et al., 2013; Zhou et al., 2015; Lan et al., 2019; Liu et al., 2022). Given the significantly higher elastic modulus of steel in contrast to that of silica gel, the deformation of the dry cabin and pipe can be deemed inconsequential, thereby identifying both as rigid bodies. Within the simulated model, the rigid body takes on the designation of the principal surface, whilst the sealant airbag is characterized as the subordinate surface.

Face-to-face contact pairs are established between airbags and rigid bodies. As shown in Fig. 2, in order to limit the deformation of the airbag in the non-radial direction, the width of the groove of the cabin is designed to be the same width as the airbag. Since the bottom of the airbag is glued to the groove of the cabin body, the tangential contact behavior between the airbag and the bottom surface of the groove is set to non-slip. The tangential contact behavior between the airbag and the groove side wall, and between the airbag and the pipeline, is set as friction contact. The contact coefficient is 0.15. In addition, by specifying a starting point for full exposure to the fluid, as shown in Fig. 2, the pressure-penetration function in ABAQUS can simulate the phenomenon of fluid penetrating two contact surfaces (simulating the water pressure). The hydraulic pressure is imposed from the initiation point to the interfacing surfaces on either side, with the bearing of pressure application aligning orthogonally to these surfaces. Load application ceases when the contact stress (P_c) at a particular node surpasses the threshold of penetration pressure (P_p).

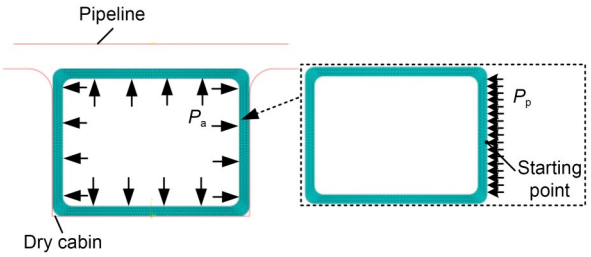

Fig. 2 Airbag meshing

The simulation procedure is articulated through three analytical stages. The initial step resolves the contact interference juxtaposing the airbag and the dry cabin. The subsequent step entails the application of internal air pressure (P_a) to the airbag, simulating its inflationary progression. In the final step, the fluid penetration function is implemented to mirror the process of escalating operating pressure (P_p) on one flank of the airbag.

As shown in Fig. 2, the airbags were suitably sliced to divide the structured mesh. Mesh-convergence studies will also be discussed below.

For the uniaxial test, please refer to Section S1 of the electronic supplementary materials (ESM). For the airbag expansion and seal pressure test, please refer to Section S2 of the ESM.

4 Simulation cases

4.1 Airbags with different physical characteristics

4.1.1 Different section shapes

As shown in Fig. 3, the most widely used airbags on the market have five different cross-sectional shapes. Different cross-section shapes produce different deformations after inflation, making the bags suitable for sealing in different working conditions. In order to select the best airbag for sealing in the arc section between the dry cabin and the pipeline, the sealing performance of airbags with different section shapes will be studied. The detailed dimensions of the airbags are shown in Fig. S4 of the ESM. The wall thickness t_a and width w_a of the airbag studied are 1.5 and 40.0 mm, respectively. The gap g_a between the top of the airbag and the pipeline is 5 mm. The airbag has a Shore hardness of 60 HA and its stress–strain data is covered in the next section. In the simulation, the airbag inflation pressure P_a is 0.4 MPa, and the penetration pressure P_p is 0.2 MPa.

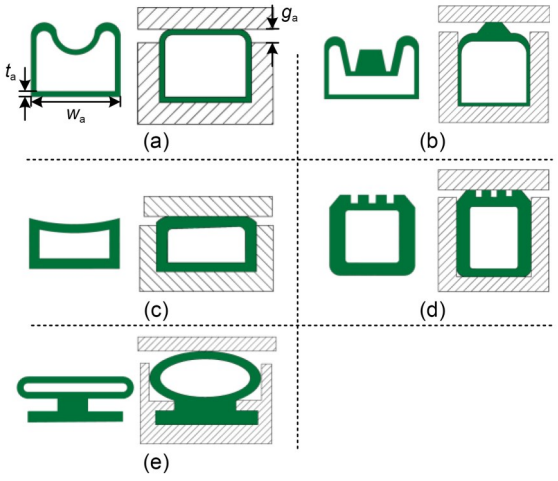

Fig. 3 Sealing airbags with different cross-sections: (a) Section-1; (b) Section-2; (c) Section-3; (d) Section-4; (e) Section-5

Fig. 3a shows cross-section-1 (S1). This type of airbag has a large expansion stroke and good sealing performance, and is suitable for the application scenario that requires a large expansion amount.

Fig. 3b shows cross-section-2 (S2). This type of airbag is a modified version of S1, and is suitable for an ultra-high expansion ratio and working conditions with large sealing gaps. Due to its high ejection ratio and slightly poor pressure resistance, it is not suitable for high-pressure sealing conditions.

Fig. 3c shows cross-section-3 (S3). This type of airbag is mainly used for radial expansion sealing and can be used as a fixture. When expanding, the contact surface is wide, the sealing effect is good, and the sealing gap is small. It has excellent pressure resistance and is widely used in all kinds of sealing situations.

Fig. 3d shows cross-section-4 (S4), which is similar to S3. This type of airbag improves the sealing performance against particles and dust with an optimized sealing surface design, and is often used for sealing pharmaceutical and papermaking equipment. It also has good pressure resistance.

Fig. 3e shows cross-section-5 (S5). This type of airbag contains a base, which is easy to fix in place and does not shift or fall off easily, and offers large expansion, suitable for sealing conditions with large expansion requirements.

4.1.2 Different hardnesses

Commercially available silicone airbags have Shore hardness between 50 and 70 HA. In order to accurately model the stress–strain constitutive model of the airbag in ABAQUS, we carried out uniaxial tensile and compression experiments on silica gel samples with Shore hardness of 50, 60, and 70 HA. Each sample had four parallel samples. Fig. 4 shows the uniaxial test data for the samples. For each curve, the area between the two dashed lines represents the distribution of the four test results. Under the same strain, the greater the hardness of the silica gel, the greater the stress, which is in line with the characteristics of the material.

According to the uniaxial test data, the specific methods to determine C_{10} and C_{01} in the Mooney-Rivlin constitutive model of airbags are as follows. σ_1 under different λ_1 is measured according to the test. $\frac{1}{\lambda_1}$ is taken as the horizontal coordinate, and $\frac{\sigma_1}{2\left(\lambda_1^2-\frac{1}{\lambda_1}\right)}$ is taken as the vertical coordinate. The test point is drawn in the coordinate system and fitted to a straight line. C_{10} is the intercept of this line, and C_{01} is the slope. Based on the fitting results, C_{10}, C_{01}, and failure stress of silica gel with three hardness levels are shown in Table 1.

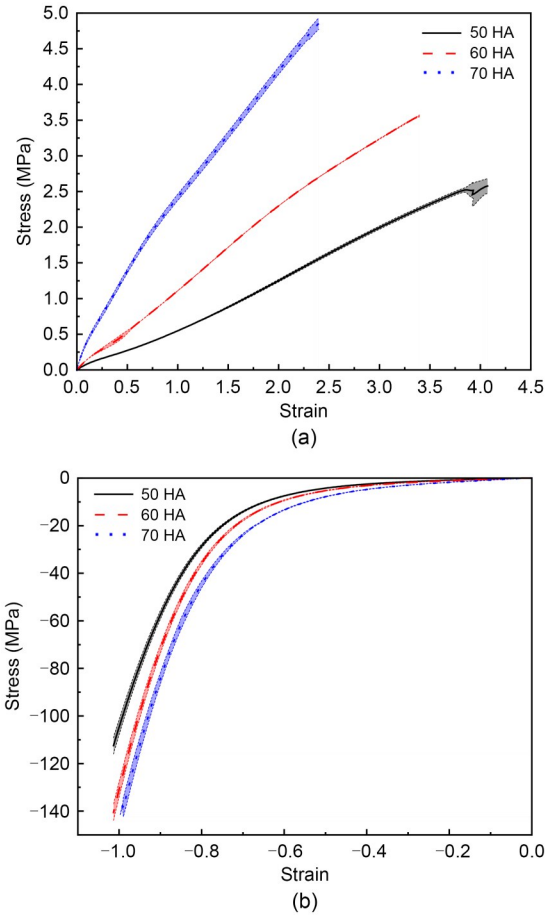

Fig. 4 Uniaxial test results for silica gel with different hardnesses: (a) uniaxial tensile; (b) uniaxial compression

Table 1 C_{10} and C_{01} of silica gel with three levels of hardness

Shore hardness (HA)	Failure stress (MPa)	C_{10}	C_{01} ($\times10^{-3}$)
50	2.55	0.299	−3.930
60	3.75	0.395	−5.217
70	4.77	0.412	−5.384

4.1.3 Different airbag wall thicknesses

The wall thickness t_a of the airbag also affects its sealing performance. Under the same inflation pressure, an airbag with thinner walls can produce greater deformation; that is, it can fill a larger gap. However, the too-low wall thickness will reduce the strength of the airbag and the corresponding reduction of pressure resistance. Therefore, in order to select the appropriate wall thickness, it was necessary to study the deformation and stress characteristics of the airbag with different wall thicknesses. The wall thickness t_a of the airbag ranged from 1.5 to 4.0 mm.

4.2 Different sealing gaps g_a

As mentioned above, in the maintenance of a curved pipe, the dry cabin and pipe will have a different coaxial situation; that is, the pipe will be eccentric relative to the arc section of the dry cabin. The fact that the dry cabin sitting on sediment will also settle unevenly exacerbates this, as shown in Fig. 5. Section 4.1 discusses the influence of airbag physical characteristics on sealing performance at g_a=5 mm.

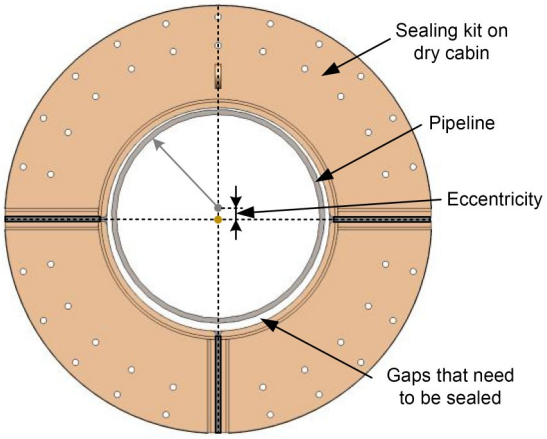

Fig. 5 Diagram of the eccentricity of the pipe relative to the dry cabin

5 Results and discussion

5.1 Mesh-convergence research

We studied mesh convergence using an airbag with a Shore hardness of 60 HA and cross-section S3. The airbag width and height are 40 and 30 mm, respectively, and the thickness is 1.5 mm. Based on the size of the airbag, we verified the functions of ABAQUS for simulating airbag inflation and pressure penetration. In the simulation, the airbag inflation pressure P_a is 0.4 MPa, and the penetration pressure P_p is 0.1 MPa. Fig. 6 shows the shapes of the airbag at three moments. As shown in Fig. 6b, the airbag expanded at a pressure of 0.4 MPa. Under the constraint of the cabin, the airbag mainly expands in the vertical direction and fills the gap between the cabin body and the pipeline. The top of the airbag contacts the pipe and creates contact stress. As shown in Fig. 6c, P_p=0.1 MPa is applied to the right side of the airbag, resulting in slight compression in the upper right corner of the expanded airbag.

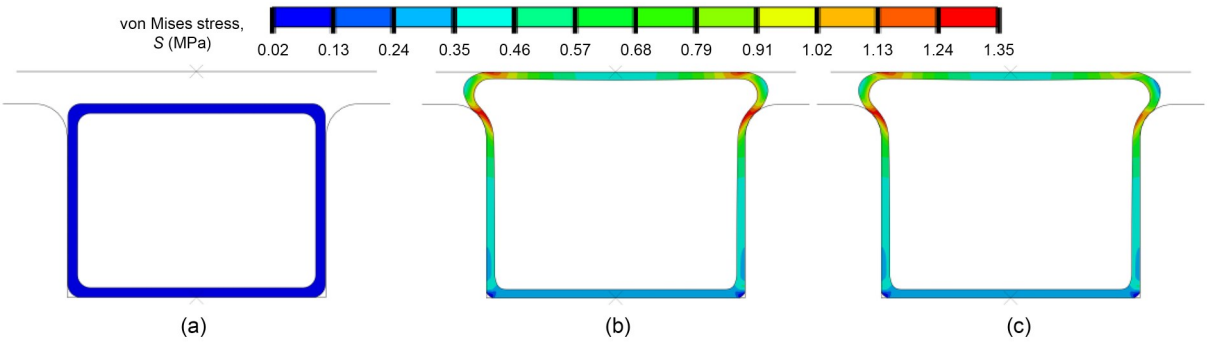

Fig. 6 von Mises stress distributions of airbag at different moments: (a) initial moment; (b) applied gas pressure P_a; (c) applied penetration pressure P_p

Fig. 7 depicts the correlation between the maximum contact stress and maximum von Mises stress with the increase of mesh number, and the specific values are tabulated in Table 2. Both the maximum contact stress and the maximum von Mises stress increase with the mesh number, while the rate of change decreases with the mesh number. When the mesh number surges from 2220 to 5394, the change rates of both the stress metrics settle at a minuscule 0.08%. This represents a substantial diminution relative to the scenario with a smaller number of meshes. Therefore, in subsequent simulation models, the mesh size of 0.3 mm is used.

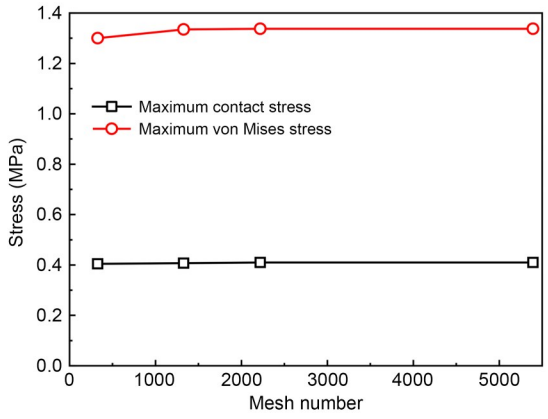

Fig. 7 Changes in maximum contact stress and maximum von Mises stress with the increase of mesh number

5.2 Influence of airbag characteristics on sealing performance

5.2.1 Influence of cross-section on sealing performance

In this section, the sealing characteristics of airbags with five kinds of section shapes are discussed. In the simulation, the P_a is 0.4 MPa, and the P_p is 0.2 MPa. More detailed operating settings are described in Section 4.1. As shown in Fig. 3, the commonly used airbags on the market have five different cross-section shapes. Airbags with different cross-section shapes produce different deformations after aeration, that is, different sealing performance. As described above, we studied this in order to select the optimal airbag for sealing the arc section between the dry cabin and the pipeline.

Fig. 8a illustrates that the peak values of contact stress generated by airbags with different cross-sections are significantly different. Due to the uneven contact surface at the top of the airbags with S2 and S4, large contact stress is generated, with similar stress magnitude. Because the top of the airbags with the other cross-sections is flat, the contact stress is small. However, the contact stress of all airbags is greater than the penetration pressure of 0.2 MPa, which meets the requirements of sealing. As shown in Fig. 8b, the uneven top surface of airbags with S2 and S4 results in stress concentration and large von Mises stress. The von

Table 2 Maximum contact stress and maximum von Mises stress corresponding to different mesh numbers

Mesh size (mm)	Mesh number	Maximum contact stress (MPa)	Rate of change (%)	Maximum von Mises stress (MPa)	Rate of change (%)
0.8	328	0.404829	–	1.30044	–
0.4	1328	0.407413	0.64	1.33502	2.66
0.3	2220	0.409558	0.53	1.33757	0.19
0.2	5394	0.409891	0.08	1.33767	0.08

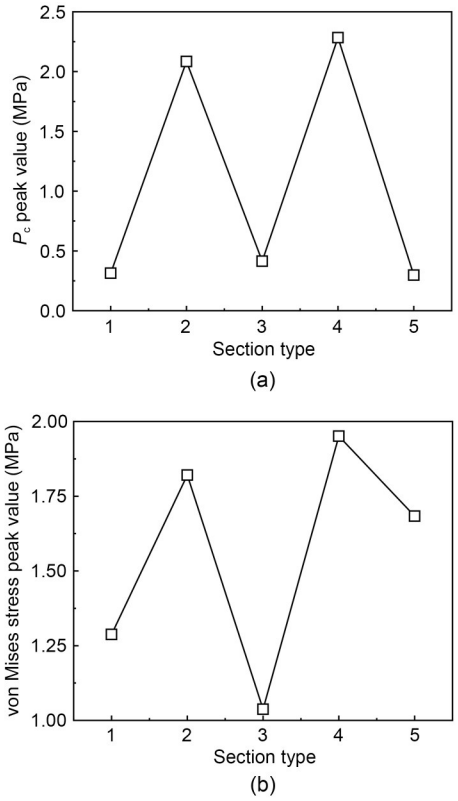

Fig. 8 (a) Contact stress peak values of airbags with different cross-sections; (b) von Mises stress peak values of airbags with different cross-sections

Mises stress of the airbag with S3 is small due to its regular shape and uniform inflation. Large von Mises stress shortens airbag life. Failure of the conventional solid seal will only result in slow penetration of the liquid. However, the destruction of the airbag will cause the seal to fail instantaneously, and the gap that was originally filled by the airbag will be immediately restored, causing a large influx of seawater into the dry cabin. Therefore, to ensure the safety of underwater operation of dry cabins, it is essential to keep von Mises stress at a low level.

Thus, comprehensively considering the contact stress and von Mises stress of the airbags with five types of cross-section, we selected airbags with S3 as the sealing tool for the dry cabin.

5.2.2 Influence of airbag hardness on sealing performance

Cross-section-5 was selected as the final airbag type in the previous section. This section takes airbag with S3 as the research object and discusses the influence of hardness on airbag sealing characteristics. The material parameters of the airbags with three hardness levels were obtained by uniaxial testing and are discussed in detail in Section 4.1.2. In the simulation, the effect of water pressure was not considered (P_p= 0 MPa).

As shown in Fig. 9a, the peak contact stress of the airbag in the part in contact with the pipeline increases with inflation pressure, and the hardness has little effect on the peak contact stress. Since the sealing mechanism of the airbag is inflation and expansion, the peak contact stress is basically equal to the air pressure. As shown in Fig. 9b, as the deformation degree of the airbag increases with the air pressure, the von Mises stress peak value also increases with the increase of inflation pressure. When the P_a is less than 0.5 MPa, the von Mises stress peak value of the hard airbag is larger. When the P_a is greater than 0.5 MPa, the von Mises stress peak of the airbag with a hardness of 50 HA becomes the maximum. As shown in Fig. 10, the airbag with a low hardness has a large deformation under

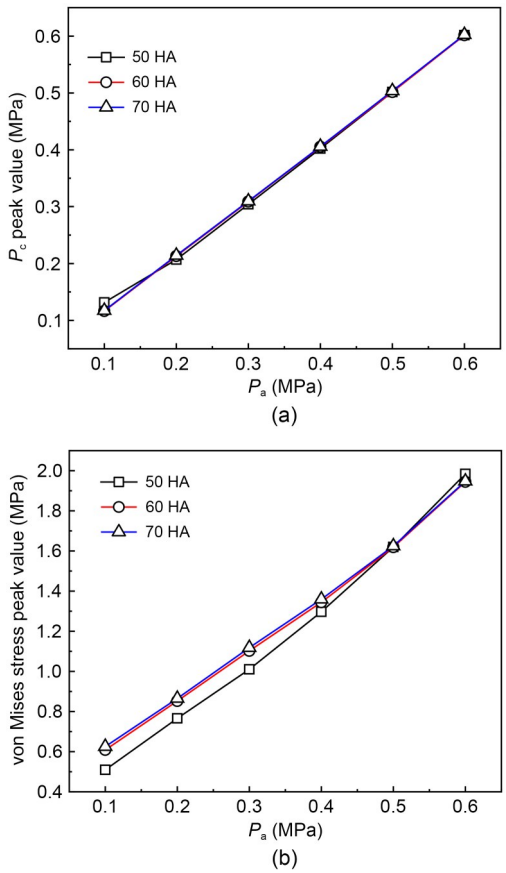

Fig. 9 Mechanical properties of airbags with three levels of hardness under different inflation pressures: (a) contact stress peak; (b) von Mises stress peak

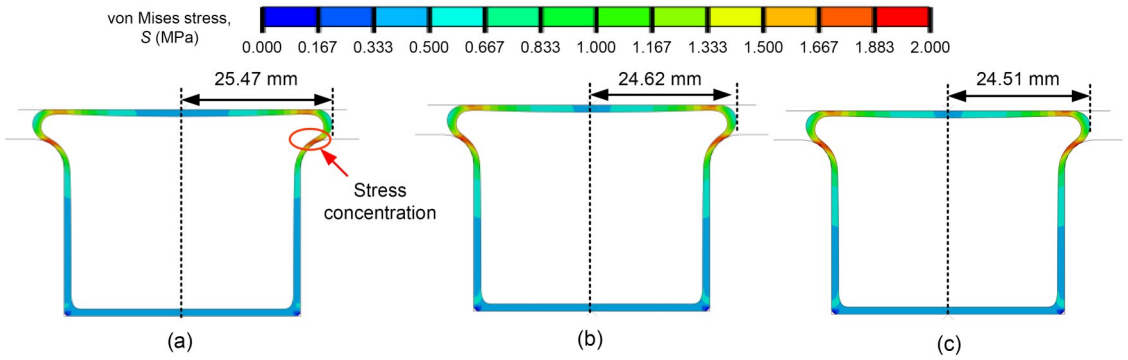

Fig. 10 von Mises stress distributions at P_a=0.6 MPa of airbags with three levels of hardness: (a) 50 HA; (b) 60 HA; (c) 70 HA

relatively large P_a, and the part in contact with the chamfer of the cabin has a large stretch, resulting in stress concentration. Greater magnitudes of von Mises stress augment the propensity for material fracturing. Additionally, significant von Mises stress levels accelerate stress relaxation within the rubber material, consequently inducing a decline in its inherent "stiffness" and leading to seal failure. Therefore, we ultimately selected the airbag with a hardness of 60 HA.

5.2.3 Influence of airbag wall thickness on sealing performance

In this section, we discuss the effect of wall thickness on the sealing characteristics of the airbag with a hardness of 60 HA. The wall thicknesses t_a tested were 1.0, 1.5, 2.0, and 2.5 mm. In the simulation, the effect of water pressure is not considered (P_p=0 MPa).

As shown in Fig. 11a, consistent with the conclusion drawn above, the peak contact stress of the airbag increases with inflation pressure. Under the same air-pressure conditions, the contact stress generated by the thicker airbag is larger, but the difference is not particularly obvious. As shown in Fig. 11b, when the inflation pressure increases, the deformation degree of the airbag increases, and the von Mises stress peak increases correspondingly. The larger the thickness of the airbag, the larger the cross-section area, and the smaller the stress under the same air pressure, so the smaller the deformation degree; that is, the smaller the von Mises stress peak value. The von Mises stress peak value showed a more obvious increasing trend with the increase of air pressure when the wall thickness of the airbag was small. The increasing trend tended to be gentle and gradually closed with increasing airbag wall thickness.

As shown in Fig. 12a, the maximum contact stress of the airbag is on both sides of the contact surface,

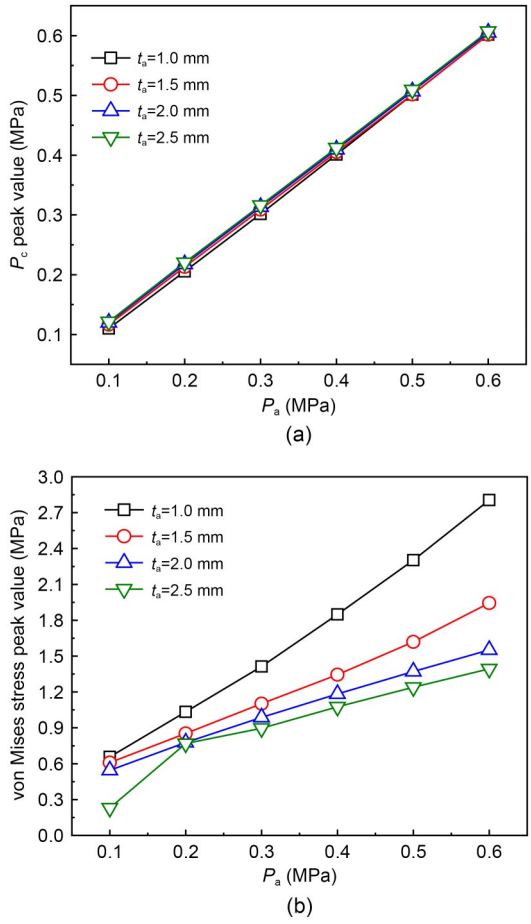

Fig. 11 Mechanical properties of airbags with four wall thicknesses under different inflation pressures: (a) contact stress peak; (b) von Mises stress peak

which is different from the contact stress distribution of the O-ring (Wu et al., 2017; Huon et al., 2022; Wu and Li, 2022). By comparing Figs. 12a and 13, it can be seen that locations with higher von Mises stress values showed higher peak contact stress values. The larger the von Mises stress, the greater the compression degree

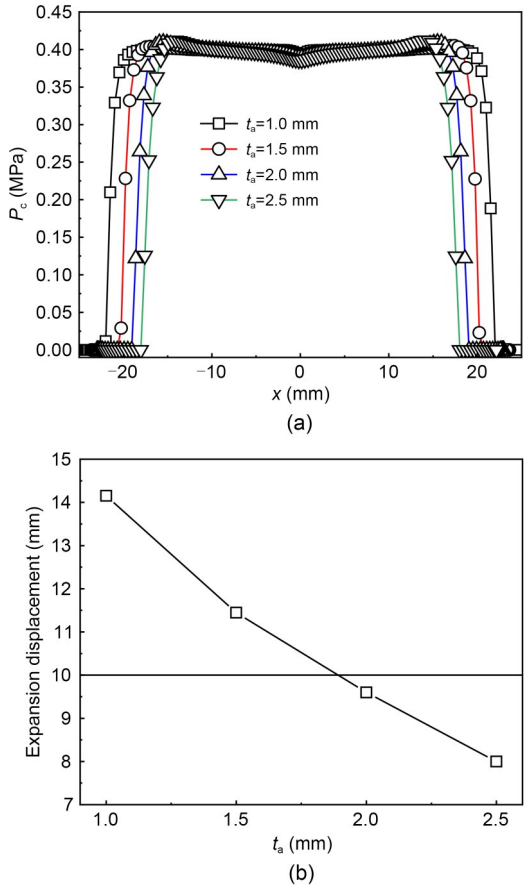

Fig. 12 (a) Contact stress distribution of airbags with four wall thicknesses; (b) expansion displacement of airbags with four kinds of wall thickness in the *y* direction at P_a= 0.2 MPa

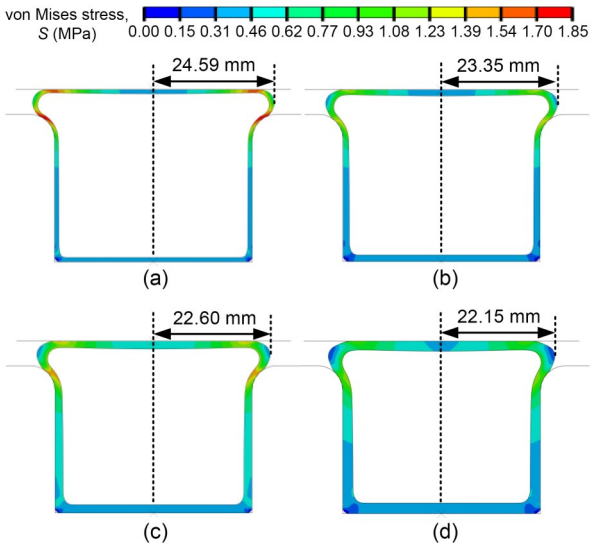

Fig. 13 von Mises stress distributions of airbags with four wall thicknesses at P_a=0.4 MPa: (a) t_a=1.0 mm; (b) t_a=1.5 mm; (c) t_a=2.0 mm; (d) t_a=2.5 mm

of the airbag, and thus the greater the contact stress between the airbag and the pipeline. The sealing surface width of an airbag with a smaller wall thickness is larger because of its better ductility. With the increase of wall thickness, the width of the sealing surface decreases, but the peak value of contact stress on both sides increases, so the sealing performance increases with wall thickness. As shown in Fig. 13, with increasing wall thickness, the deformation degree of the airbag decreases continuously, and the overall von Mises stress of the airbag shows a downward trend. With regard to contact stress and von Mises stress, the performance of airbags with large wall thicknesses is better. However, Fig. 12b demonstrates that the large wall thickness results in poor ductility of the airbag, and the airbag not being able to expand to fill a larger gap. When the air pressure is 0.2 MPa, the expansion height of the airbag with a wall thickness of 2.5 mm is much less than 10 mm, which is the maximum gap between the pipe and the cabin body. When the pressure at a working water depth of 0.4 MPa is taken into consideration, the total pressure of 0.6 MPa is close to the maximum working pressure of the air compressor. Therefore, an airbag with a wall thickness of 2.5 mm is not conducive to filling the gap.

To ensure good gap-filling capacity and low von Mises stress, we selected the airbag with a wall thickness of 2.0 mm.

5.3 Airbag sealing performance in different gaps

Because a curved pipe is eccentric relative to the arc section of the dry cabin, the distance (seal gap) between the top surface of the airbag and the pipe will be different in various circumferential positions. Therefore, it is necessary to clarify the relationship between the inflation pressure and different sealing gaps and study the sealing characteristics of the airbag under a time-varying gap. Above, it was determined to use an airbag with a cross-section of S3, a hardness of 60 HA, and a wall thickness of 2.0 mm.

After the dry cabin sits at the bottom of 40 m water depth, the ambient pressure of seawater is 0.4 MPa, and the uninflated airbag is compressed. Therefore, it is necessary to fill the airbag with 0.4 MPa of gas to restore it to its natural state. On the basis of 0.4 MPa, a gasbag with larger gas pressure will expand and fill the gap between the pipe and the dry cabin. As shown in Fig. 14a, the required inflation pressure increases as

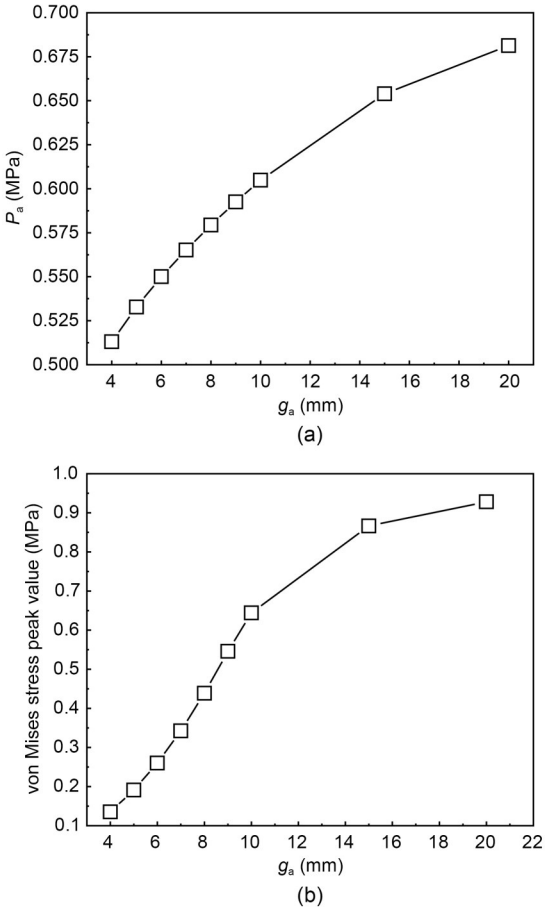

Fig. 14 (a) Air pressures required for the airbag to form a seal under different gap conditions; (b) von Mises stress peak values after the airbag formed a seal under different gap conditions

the gap widens. The increasing trend tends to be flat with the widening of the gap. Inflation of the airbag by 5 mm requires 0.533 MPa, and 20 mm requires 0.681 MPa. The data in Fig. 14a can guide the control of airbag air pressure during the actual operation of a dry cabin. As shown in Fig. 14b, the von Mises stress peak value increased along with airbag expansion, and the trend was similar to that of air pressure. However, the von Mises stress of the airbag was less than 1 MPa, which was far less than the failure stress of the uniaxial test (2.55 MPa).

5.4 Airbag test

5.4.1 Airbag inflation height test

In order to verify the accuracy of the airbag elastic deformation constitutive model and the accuracy of simulating airbag inflation deformation using ABAQUS, we tested the expansion of customized airbags under different air pressures, as shown in Fig. 15a. Fig. 15b illustrates that the experimental results are consistent with the simulation results. When the air pressure is in the range of 0.015–0.025 MPa, the experimental results are in agreement with the simulation results. When the air pressure is low or high, the error between the two is significant, with a maximum difference of 0.4 mm. In summary, the test results verify the rationality of the simulation results.

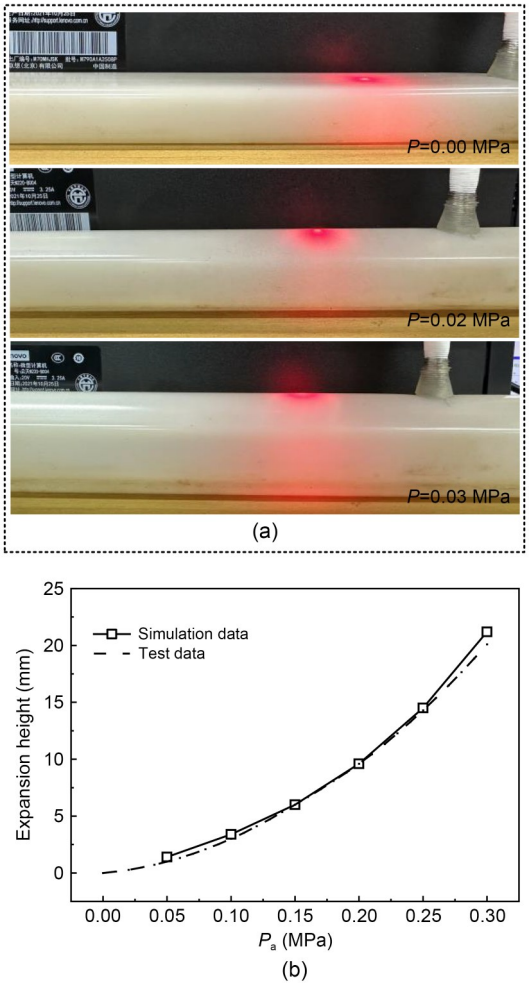

Fig. 15 (a) Diagram of airbag inflation; (b) relationship between airbag inflation height and air pressure

5.4.2 Airbag pressure-bearing capacity test

In order to verify the accuracy of the simulation results, we carried out a pressure test on the selected airbag. The inner diameter of the outer cylinder of the seal test cabin is 410 mm, the outer diameter of the inner cylinder is 340 mm, and the initial height of the

airbag is 30 mm (Fig. S3). Therefore, the gap to be filled by the airbag is 5 mm, which is the same as the gap in the simulation. The width of the airbag is 40 mm, the height is 30 mm, the thickness is 2 mm, the hardness is 60 HA, and the diameter is 410 mm (the same as the inner diameter of the outer cylinder).

To ascertain the potential leakage within the experimental cabin, the pressurization process was halted upon reaching a specific pressure threshold, as shown in Fig. 16a, followed by a periodic observation to detect any notable depressurization within 30 s. The experimental cabin underwent pressurization at a rate of 0.1 MPa/s.

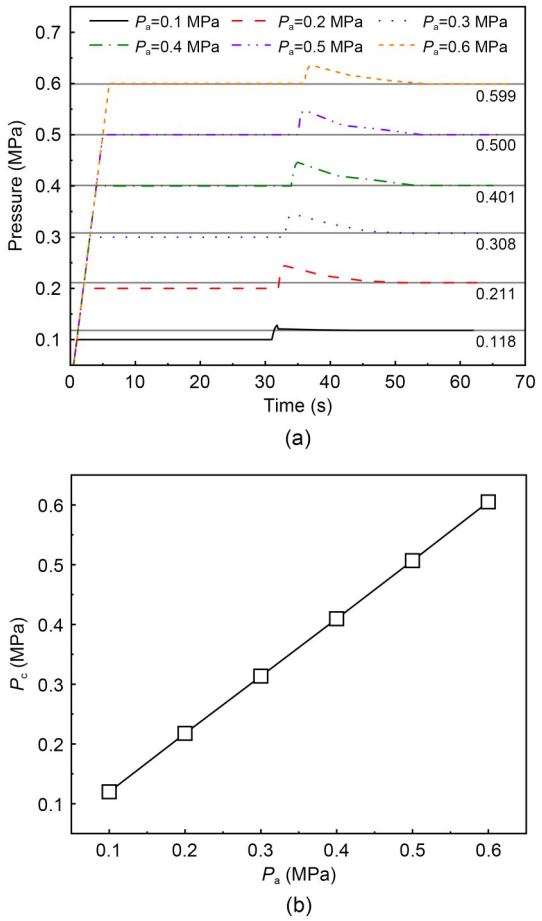

Fig. 16 (a) Pressure-bearing capacity test results of the airbag under different air pressures; (b) simulation results of the peak contact stress generated by the airbag under different air pressures

During the test, the airbags were filled with gases of 0.1, 0.2, 0.3, 0.4, 0.5, and 0.6 MPa in sequence. When the pressure in the test cabin was lower than that of the airbag, it increased continuously over time. When the cabin pressure was higher than that of the airbag, it dropped to a level equivalent to the airbag pressure after pressurization was stopped. After testing, the pressure-bearing capacities of the airbag under different inflation pressures were 0.118, 0.211, 0.308, 0.401, 0.500, and 0.599 MPa, corresponding to the gas levels given above.

Fig. 16b shows the simulation results of the peak contact stress, i.e., 0.120, 0.218, 0.313, 0.410, 0.507, and 0.605 MPa, generated by the airbag under different inflation pressures. The differences between these measurements and the test results were 1.5%, 3.0%, 1.7%, 2.1%, 1.3%, and 1.0%, respectively. The small differences can still explain the accuracy of the simulation calculation.

6 Conclusions

In this paper, we proposed applying a non-standard airbag to seal a dry cabin for the maintenance of a submarine pipeline. We used ABAQUS finite element software to study the influence of the physical characteristics of the airbag on its deformation characteristics and sealing performance. In addition, we studied the adaptive sealing mechanism of the airbag under the time-varying gap condition. Ultimately, a rectangular airbag with a hardness of 60 HA and wall thickness of 2.0 mm was selected after comprehensively considering airbag stiffness, gap-filling capacity, and von Mises stress. The conclusions are as follows:

(1) Of five cross-section shapes, the rectangular cross-section resulted in the minimum von Mises stress under the premise of satisfying the seal, which can improve the safety of airbag operation.

(2) The peak contact stress of the airbag is close to the level of the air pressure, so the hardness of the airbag has almost no effect on the peak contact stress. Airbag hardness had a slight effect on the von Mises stress.

(3) The contact stress generated by a thicker airbag is greater, so sealing performance increases with wall thickness. Higher wall thickness decreases the deformation degree, and the von Mises stress shows a downward trend. However, higher wall thickness results in poorer ductility of the airbag, and an inability to expand to fill larger gaps.

(4) Under time-varying gap conditions, as the gap widens, the required gas pressure also increases. The

von Mises stress peak value increases with the airbag expansion, and the trend is similar to that of the gas pressure. The simulated relationship between the gap and the air pressure can guide the air-pressure control of an airbag during the actual operation of a dry cabin.

(5) The maximum difference between the simulation results and those of the airbag expansion test is only 0.4 mm, and the maximum difference between the pressure results of the airbag and the simulation results is only 3.0%, which indicates that ABAQUS can be used to accurately study the inflation deformation and sealing characteristics of airbags.

Acknowledgments

This work is supported by the Eyas Program Incubation Project of Zhejiang Provincial Administration for Market Regulation (No. CY2023107), the PhD Scientific Research and Innovation Foundation of Sanya Yazhou Bay Science and Technology City (No. HSPHDSRF-2023-04-003), the Scientific Research Fund of Zhejiang Provincial Education Department, China (No. Y202353239), and the Zhoushan Field Scientific Observation and Research Station for Marine Geo-hazards, China Geological Survey (No. ZSORS-22-14).

Author contributions

Jin GUO designed the research. Xinghui TAN and Hai ZHU processed the corresponding data. Jin GUO and Shidi JIN wrote the first draft of the manuscript. Yuanjie CHEN and Jie CHEN helped to organize the manuscript. Jiawang CHEN and Ruiduo YIN revised and edited the final version.

Conflict of interest

Jin GUO, Xinghui TAN, Hai ZHU, Jiawang CHEN, Shidi JIN, Yuanjie CHEN, Jie CHEN, and Ruiduo YIN declare that they have no conflict of interest.

References

Animah I, Shafiee M, 2018. Condition assessment, remaining useful life prediction and life extension decision making for offshore oil and gas assets. *Journal of Loss Prevention in the Process Industries*, 53:17-28. https://doi.org/10.1016/j.jlp.2017.04.030

Badida P, Balasubramaniam Y, Jayaprakash Y, 2019. Risk evaluation of oil and natural gas pipelines due to natural hazards using fuzzy fault tree analysis. *Journal of Natural Gas Science and Engineering*, 66:284-292. https://doi.org/10.1016/j.jngse.2019.04.010

Berge M, Birdsall L, Erickson A, et al., 2008. Underwater habitat clamp (UHC): an innovative partnership in underwater pipeline repair. Proceedings of the 7th International Pipeline Conference, p.193-200. https://doi.org/10.1115/IPC2008-64607

Chen J, Zheng YX, Zhong XK, et al., 2023. Working mechanism and testing of emergency reinforced airbag used for blocking in tunnels. *Tunnelling and Underground Space Technology*, 138:105201. https://doi.org/10.1016/j.tust.2023.105201

Chen Y, Chen GP, He H, 2019. Simulation of a folded airbag inflating underwater with IMM method. *IOP Conference Series: Materials Science and Engineering*, 531:012004. https://doi.org/10.1088/1757-899X/531/1/012004

Cui KB, Qin JQ, Di CC, et al., 2013. Finite element analysis and simulation of the sealing performance of Y-ring rubber seal. *Applied Mechanics and Materials*, 444-445:1379-1383. https://doi.org/10.4028/www.scientific.net/AMM.444-445.1379

Dong JH, Liu SH, Zhang H, et al., 2021. Experiment and simulation of a controllable multi-airbag sealing disc of pipeline inspection gauges (PIGs). *International Journal of Pressure Vessels and Piping*, 192:104422. https://doi.org/10.1016/j.ijpvp.2021.104422

Drumond GP, Pasqualino IP, Pinheiro BC, et al., 2018. Pipelines, risers and umbilicals failures: a literature review. *Ocean Engineering*, 148:412-425. https://doi.org/10.1016/j.oceaneng.2017.11.035

Eisenreich N, Neutz J, Seiler F, et al., 2007. Airbag for the closing of pipelines on explosions and leakages. *Journal of Loss Prevention in the Process Industries*, 20(4-6):589-598. https://doi.org/10.1016/j.jlp.2007.04.030

Fleury G, Schofield R, 1979. Dry habitat connections and repairs of subsea pipe-line and structures. Proceedings of the Middle East Technical Conference and Exhibition. https://doi.org/10.2118/7770-MS

Gaudiano AV, 1975. A summary of 26 underwater welding habitat jobs. Proceedings of the Offshore Technology Conference. https://doi.org/10.4043/2302-MS

Gucma L, Zalewski P, 2003. Damage probability of offshore pipelines due to anchoring ships. *Polish Maritime Research*, 10(4):6-12.

Guo J, Zhou QX, Tan XH, et al., 2024. Study on sealing performance and optimization design of a new type non-standard seal strip of submarine pipeline maintenance dry cabin. *Ocean Engineering*, 292:116508. https://doi.org/10.1016/j.oceaneng.2023.116508

Huon C, Tiwari A, Rotella C, et al., 2022. Air, helium and water leakage in rubber O-ring seals with application to syringes. *Tribology Letters*, 70(2):35. https://doi.org/10.1007/s11249-022-01574-7

Jiang LM, Zhang YH, Huang ZA, et al., 2012. Experimental study of fast sealing airbag in simulating tunnel. *Procedia Engineering*, 45:780-785. https://doi.org/10.1016/j.proeng.2012.08.239

Lan WJ, Wang HX, Zhang X, et al., 2019. Sealing properties and structure optimization of packer rubber under high pressure and high temperature. *Petroleum Science*, 16(3):632-644. https://doi.org/10.1007/s12182-018-0296-0

Lee Toups E, Morrison RJ, Harper RJ, 2021. Development of a micro-habitat hyperbaric welding system. Proceedings of the Abu Dhabi International Petroleum Exhibition & Conference.

https://doi.org/10.2118/207602-MS

Li XH, Chen GM, Zhu HW, 2016. Quantitative risk analysis on leakage failure of submarine oil and gas pipelines using Bayesian network. *Process Safety and Environmental Protection*, 103:163-173. https://doi.org/10.1016/j.psep.2016.06.006

Liu Y, Qian LQ, Zou JY, et al., 2022. Study on failure mechanism and sealing performance optimization of compression packer. *Engineering Failure Analysis*, 136:106176. https://doi.org/10.1016/j.engfailanal.2022.106176

Ma L, Liu SM, Wei GM, et al., 2022. Dynamic response characteristics of a sealing airbag under different impact types and impact pressures. *ACS Omega*, 7(43):38589-38599. https://doi.org/10.1021/acsomega.2c04043

Mao DF, Chu G, Yang L, et al., 2015. Deepwater pipeline damage and research on countermeasure. *Aquatic Procedia*, 3:180-190. https://doi.org/10.1016/j.aqpro.2015.02.209

Mooney M, 1940. A theory of large elastic deformation. *Journal of Applied Physics*, 11(9):582-592. https://doi.org/10.1063/1.1712836

Pratt JA, Priest T, Castaneda CJ, 1997. Offshore Pioneers: Brown & Root and the History of Offshore Oil and Gas. Elsevier, Amsterdam, the Netherlands. https://doi.org/10.1016/B978-0-88415-138-8.X5036-4

Rivlin RS, 1948. Large elastic deformations of isotropic materials IV. Further developments of the general theory. *Philosophical Transactions of the Royal Society A: Mathematical, Physical and Engineering Sciences*, 241(835):379-397. https://doi.org/10.1098/rsta.1948.0024

Rivlin RS, Saunders DW, 1951. Large elastic deformations of isotropic materials VII. Experiments on the deformation of rubber. *Philosophical Transactions of the Royal Society A: Mathematical, Physical and Engineering Sciences*, 243(865):251-288. https://doi.org/10.1098/rsta.1951.0004

Tronskar JP, Lee CG, 2016. Cofferdam and hyperbaric "live" repair of gas pipeline leaks. Proceedings of the ASME 35th International Conference on Ocean, Offshore and Arctic Engineering. https://doi.org/10.1115/OMAE2016-55077

Vernon T, Werner B, 2009. Authentic innovation: the role of apprenctice learning in engineering education. Proceedings of the ASME International Mechanical Engineering Congress and Exposition. https://doi.org/10.1115/IMECE2009-10753

Wu D, Wang SP, Wang XJ, 2017. A novel stress distribution analytical model of O-ring seals under different properties of materials. *Journal of Mechanical Science and Technology*, 31(1):289-296. https://doi.org/10.1007/s12206-016-1231-1

Wu JB, Li L, 2022. Influence of ambient pressure on sealing performance of O-ring in deep-sea hydraulic system. *Ocean Engineering*, 245:110440. https://doi.org/10.1016/j.oceaneng.2021.110440

Yang YS, Khan F, Thodi P, et al., 2017. Corrosion induced failure analysis of subsea pipelines. *Reliability Engineering & System Safety*, 159:214-222. https://doi.org/10.1016/j.ress.2016.11.014

Zhou SM, Chen P, Shi Y, 2015. Analysis on sealing performance for a new type of rubber saddle-shaped sealing ring based on AQAQUS. *Procedia Engineering*, 130:1000-1009. https://doi.org/10.1016/j.proeng.2015.12.252

Electronic supplementary materials

Sections S1 and S2, Figs. S1–S4